Exploration of BioMat-X

Open Exploration

Open Access Original Article

Nanoparticle-functionalized acrylic bone cement for local therapeutic delivery to spine metastases

Ateeque Siddique, Mansoureh Mohseni Garakani, Megan E. Cooke, Michael H. Weber, Derek H. Rosenzweig*

Injury, Repair & Recovery Program, Research Institute of the McGill University Health Centre, Montreal, Quebec H3G 1A4, Canada

***Correspondence:** Derek H. Rosenzweig, Injury, Repair & Recovery Program, Research Institute of the McGill University Health Centre, Montreal, Quebec H3G 1A4, Canada. derek.rosenzweig@mcgill.ca

Academic Editor: Dennis Douroumis, University of Greenwich, UK

Received: December 31, 2023 **Accepted:** March 20, 2024 **Published:** April 28, 2024

Cite this article: Siddique A, Garakani MM, Cooke ME, Weber MH, Rosenzweig DH. Nanoparticle-functionalized acrylic bone cement for local therapeutic delivery to spine metastases. Explor BioMat-X. 2024;1:135–57. https://doi.org/10.37349/ebmx.2024.00010

Abstract

Aim: Polymethylmethacrylate bone cement is often used to reconstruct critical-sized defects generated by the surgical resection of spinal metastases. Residual tumor cells after a resection can drive recurrence and destabilization. Doxorubicin (DOX) is a common chemotherapeutic drug with unwanted side-effects when administered systemically. Mesoporous silica nanoparticles (NPs) are gaining attention for targeted drug delivery to bypass the negative side effects associated with systemic drug administration. An NP-functionalized cement was developed for the local release of DOX and its ability to suppress cancer cells was tested.

Methods: DOX was loaded onto NPs which were then mixed into the cement. Static contact angles were measured. Drug release profiles were obtained over a period of 4 weeks. Cement constructs were incubated with two-dimensional (2D) cultures of human bone-marrow derived mesenchymal stem cells and human osteoblasts, as well as 2D and three-dimensional (3D) cultures of breast and prostate cancer cell lines. Cell metabolic activity and viability were evaluated. Cell migration and spheroid growth of cancer cell lines were assessed in collagen-coated spheroid cultures.

Results: NPs were homogenously dispersed and did not alter the mechanical strength nor the wettability of the cement. A sustained DOX release profile was achieved with the addition of NPs to the bone cement. The release profile of DOX from NP cement may be modified by varying the amount of the drug loaded onto the NPs and the proportion of NPs in the cement. Cancer cells treated with the cement constructs showed a dose- and time-dependent inhibition, with minimal toxicity against healthy cells. Cancer cell migration and spheroid growth were impaired in 3D culture.

Conclusions: NPs were shown to be essential for sustained DOX release from bone cement. DOX-loaded NP cement can inhibit cancer cells and impair their migration, with strong potential for *in vivo* translation studies.

Keywords

Polymethylmethacrylate, mesoporous silica nanoparticles, chemotherapeutics, local delivery, three-dimensional culture

Introduction

The spinal column is the most common skeletal location of cancer metastasis. Spinal metastases occur in 20–40% of all cancer patients, originating primarily from breast, prostate, lung, and kidney cancers [1–3]. About 20% of spinal metastases patients are symptomatic, including pain and neurological dysfunction due to instability and epidural spinal cord compression (ESCC). Spinal metastases result in lesions in the affected vertebrae which can cause pathologic compression fractures due to the decreased load-bearing capacity of the spine [1, 2, 4]. The prevalence of spinal metastases is expected to increase with patients living longer due to improving detection and medical/surgical treatment for many cancers [4]. Furthermore, the overall postoperative survival for patients undergoing surgery for spinal metastases has improved significantly in the last 20 years [5]. Thus, it represents an increasingly important oncologic challenge. The treatment of spinal metastases aims to relieve pain, preserve neurological function, maintain the spine's mechanical stability, and improve overall patient quality of life. Medical treatment can include hormonal therapy for lesions secondary to breast and prostate cancer, chemotherapy, corticosteroids to treat inflammation, bisphosphonates to prevent bone resorption, and analgesia to relieve pain [4, 6]. Recent advances in stereotactic radiosurgery allow for the precise targeting of spinal metastases, delivering effective doses of radiation in cases of limited epidural compression. However, surgical decompression is required for higher-grade ESCC [7].

The surgical removal of spine metastases may be achieved through en bloc resection (wide excision margins to remove the tumor in a single piece), curettage/piecemeal (removal by pieces with no clearly defined margins), or a partial palliative resection for spinal cord decompression [8, 9]. Additionally, percutaneous vertebroplasty and kyphoplasty are minimally invasive vertebral augmentation procedures used to stabilize painful pathologic compression fractures [2, 6]. Although the risk of complications may be high, surgery for spinal metastases provides pain relief and neurological improvement [3]. Polymethylmethacrylate (PMMA) bone cement is commonly used for the reconstruction of the vertebral body post-resection as it is widely available, inexpensive, mechanically strong, and conforms to the shape of the bone when inserted [10]. However, the risk of cancer recurrence remains after a resection. The median time to recurrence for isolated spinal metastatic tumors is 24 months when an en bloc resection is performed, with the risk of recurrence increasing when an intralesional curettage is performed [11]. One study determined the local recurrence rate to be 14% in patients who received a percutaneous PMMA vertebroplasty to treat spinal metastases secondary to breast cancer (mean follow-up time of 42 months) [12]. In another study, one in six (17%) patients who underwent an en bloc resection experienced a local recurrence. Furthermore, most recurrences were diagnosed 2 years or more after the initial surgery [13].

Studies have investigated bone cement formulations containing antibiotics for the control of local infections in orthopedic applications since the 1970s. PMMA is most often mixed with the antibiotic vancomycin, and clinical outcomes are favourable for infection control [14]. Although these antibiotic PMMA cements are commercially available for clinical use, they are limited in their ability to control the release rate of the drugs and mixing the antibiotic powders directly into the cement can decrease its mechanical properties [15–17]. In the same way antibiotics have been mixed into PMMA for infection control, there is interest in developing PMMA cements loaded with chemotherapeutics for decreasing the rate of local tumor recurrence in bone related cancers. To date, most studies have mixed chemotherapeutics such as doxorubicin (DOX), methotrexate, and cisplatin, directly into the PMMA powder [18, 19]. In these studies, only 5–20% of the drugs mixed into the cement were eluted with most of the release occurring within 24 h, likely due to the surface burst release effect, since PMMA is non-biodegradable [20].

To increase antibiotic elution from PMMA cement, researchers have incorporated additives including borosilicate glass, nanotubes, mesoporous silica nanoparticles (NPs), polycaprolactone (PCL) and polyethylene glycol (PEG). With these additives, an increase in the drug elution occurs [21–25]. However, soluble fillers such as PCL, PEG, or even the drug powders themselves, are porogens that decrease the mechanical strength of PMMA, making it unsuitable for load-bearing applications [23, 26]. One study determined that with the incorporation of 8.15% w/w mesoporous silica NPs into PMMA bone cement, gentamicin elution was significantly enhanced without a negative impact on the cement's mechanical properties [25]. More recently, a PMMA composite with 15% w/w γ-cyclodextrin polymeric microparticles was used to enhance DOX release, with 100% release in 100 days. However, the compressive strength fell below the minimum threshold according to the American Society for Testing and Materials (ASTM) F451-16 and International Organization for Standardization (ISO) 5833:2002 standards [27]. To our knowledge, studies investigating PMMA composites as a chemotherapeutic delivery device are limited. As side effects of systemic chemotherapy administration are common (e.g., DOX-induced cardiotoxicity [28]), such a cement would function as an adjuvant therapeutic device with the potential to bypass negative side effects associated with high doses of systemic chemotherapy administration [29].

There is growing interest in the application of mesoporous silica NPs as drug carriers due to their high surface area, chemical stability, modifiable pore size, and ability to be functionalized [30]. In this study, a PMMA cement functionalized with DOX-loaded NPs was developed for a sustained drug release. Its mechanical strength and in vitro efficacy was evaluated against MDA-MB-231 breast cancer and C4-2B prostate cancer cell lines in both two-dimensional (2D) culture and three-dimensional (3D) tumor spheroid cell culture models. In addition, the cement's toxicity was assessed against human bone-marrow derived mesenchymal stem cells (hbmMSCs) and human osteoblasts. Our work is the first to investigate the application of mesoporous silica NP technology to PMMA bone cement for local chemotherapy drug delivery. Such NP-functionalized cements could be used to deliver a local dose of chemotherapeutics to lower the risk of recurrence after a spinal tumor resection surgery and improve patient outcomes.

Materials and methods

NP DOX loading

Commercially available mesoporous silica NPs with a diameter of 500 nm and a pore size of 2 nm were used (Sigma-Aldrich, #805890). NPs were weighed and placed in glass scintillation vials with 1 mL of phosphate-buffered saline (PBS; Gibco, #10010). The vials were placed in an ultrasonication ice water bath for 2 h to suspend the NPs. Following sonication, DOX hydrochloride (DOX; Sigma-Aldrich, #44583) solutions prepared in 1 mL of PBS were added to the vials to achieve final concentrations of 0, 40, 80, 120, and 240 μmol/L of DOX. The vials were placed on a nutating mixer (fixed speed of 24 rotations per minute) for 24 h at room temperature to allow the drug to be adsorbed into the NPs. The following day, the DOX-NP solutions were transferred to 2 mL Eppendorf tubes and centrifuged at 10,000 rpm for 3 min, aggregating the NPs into a pellet. The supernatant was removed and stored to quantify the concentration of unbound DOX. The pellet of DOX-loaded NPs was then dried overnight in a 37°C oven.

NP-cement preparation

To prepare the cement, the dried NP pellet was crushed and thoroughly mixed into approximately 0.326 g of SmartSet HV bone cement powder (DePuy, #3092040). To the NP-cement powder, 167.2 μL (0.154 g) of liquid methylmethacrylate monomer pre-cooled to 4°C was added and mixed thoroughly for approximately 30 s with a spatula. Once the cement achieved a workable consistency, it was mixed on the palm of the hand until it was no longer adhering to the glove, for about 60 s. The mixed cement was then placed into a 1 mL BD Tuberculin Slip Tip syringe (BD, #309659) and was extruded to form a log of cement. A 3D-printed jig was used to cut the malleable cement rod into cylinders of approximately 3 mm in height and 2 mm in diameter. For *in vitro* assays, the cement pods were placed under an ultraviolet light overnight for sterilization. Cement with DOX without NPs (Ø NP) was prepared with an equivalent of the 120 μmol/L concentration (240 nmol). The DOX solution was mixed into the cement powder and dried on a hotplate

before the liquid fraction was added and the cement was mixed. The various cement compositions are outlined in Table 1. Note that the % w/w measurements are in reference to the total mass of the cement formulation.

Table 1. Cement formulations

Sample	Cement powder (g)	Cement liquid (mL)	NPs (mg)		DOX loaded (nmol)	DOX loaded (% w/w)
			2% w/w	8% w/w		
Blank	0.326	0.167	0	0	0	0
Ø NP	0.326	0.167	0	0	240	0.027
0 μmol/L	0.326	0.167	10	40	0	0
40 μmol/L	0.326	0.167	10	40	80	0.008
80 μmol/L	0.326	0.167	10	40	160	0.017
120 μmol/L	0.326	0.167	10	40	240	0.025
240 μmol/L	0.326	0.167	10	40	480	0.050

Static contact angle measurements

Static contact angles (SCA) were measured at room temperature using a tensiometer (OCA DataPhysics, model TBU 90E). Cement samples (blank, 2% w/w NPs, 8% w/w NPs) were placed into the device and 2 μL droplets of MilliQ water were placed on the surface with a microsyringe. Average values along with standard deviations (SD) of SCAs were evaluated using the SCA20U software provided by the manufacturer.

Drug release kinetics

The cylindrical cement pods were weighed, and their dimensions were measured with calipers to the nearest 0.02 mm before being placed into 2 mL Eppendorf tubes with 500 μL of PBS to fully submerge the cement pods. The time of PBS addition was considered the zero timepoint, namely, day 0. After 24 h (day 1), 250 μL of PBS was removed and stored to quantify the concentration of DOX. The volume withdrawn (250 μL) was replenished with fresh PBS to regain the total volume of 500 μL. This was repeated on days 4, 7, 14, 21, and 28. The basis of measuring the concentration from the aliquots of withdrawn PBS relied on the autofluorescence of DOX (excitation: 470 nm, emission: 585 nm). The fluorescence intensity was measured with a TECAN Infinite M200 Pro microplate reader (TECAN, Männedorf, Switzerland) and the concentrations were interpolated from a standard curve. The cumulative DOX concentrations were calculated recursively using the following equation:

$$Cumulative\ [DOX] = [DOX]_t + \frac{Volume\ withdrawn}{Total\ volume} \times [DOX]_{t-1}$$

Where, $[DOX]_t$ is the concentration of DOX at time t and $[DOX]_{t-1}$ is the concentration of DOX at time prior to t (previous timepoint).

Mechanical compression testing

To evaluate the mechanical properties of the cement, cylindrical samples were prepared with a diameter of 6 mm and a height of 12 mm, as per the ASTM F451-16 and ISO 5833:2002 standards. Cement without NPs (blank) and with 8% w/w NPs was mixed and molded into cylinders using a cardboard tube with an inner diameter of 6 mm. Once cured, the tubing was removed, and the ends were sanded square to the correct height using 320 grit sandpaper. The dimensions were measured to the nearest 0.02 mm using calipers. Uniaxial compression testing was performed on an Instron 1362 (Instron, Norwood, Massachusetts, USA) with a ReNew MTS controller (MTS Systems Corporation, Eden Prairie, Minnesota, USA) and a 20 kN load cell at an unconfined compression rate of 20 mm/min. The Young's moduli (moduli of elasticity) were calculated as the slopes of the linear portions of the stress-strain curves. The ultimate compression strengths were determined from the upper yield point loads on the stress-strain curves.

Scanning electron microscopy

Samples were prepared as above without DOX and cured. They were then mounted in varying orientations onto aluminum stubs using double-sided carbon tape. Samples were then coated with a 4 nm layer of platinum using a ACE600 high resolution sputter coater (Leica Microsystems) before being imaged using an FEI Quanta 450 ESEM (Thermo Fisher Scientific, Saint Laurent, QC).

Cell lines and *in vitro* efficacy assays

The cell lines employed in this study were the triple-negative MDA-MB-231 breast cancer cell line provided by Professor M. Park's laboratory at McGill University and the bone metastatic C4-2B prostate cancer cell line. To obtain DOX dose-response curves for these cell lines, 20,000 cells in the log phase of growth were seeded in 48-well tissue culture plates. MDA-MB-231 and C4-2B cells were seeded in Dulbecco's modified Eagle medium (DMEM; Gibco, #12430062) and Roswell Park Memorial Institute (RPMI) 1640 (Gibco, #11835055), respectively, supplemented with 10% heat-inactivated fetal bovine serum (FBS; Gibco, #12483020) and 1% penicillin-streptomycin (Gibco, #15140122). The following day, the cell medium was removed and replaced with a low-serum (1% FBS) media containing the following concentrations of DOX: 0 (PBS vehicle control), 0.001, 0.01, 0.05, 0.1, 0.5, 1, 5, 10, and 100 μmol/L. AlamarBlue (Invitrogen, #DAL1100) resazurin reduction assays were performed after 3 days and 7 days of DOX treatment to determine metabolic activity compared to control. Briefly, cell medium was removed and a 10% AlamarBlue solution in low-serum medium was added and the plates were incubated at 37°C for 4 h. The resorufin fluorescence was quantified using the TECAN fluorescence microplate reader (excitation: 560 nm, emission: 590 nm).

To determine the *in vitro* efficacy of the DOX cement against tumor cells in a 2D monolayer culture, the cement constructs loaded with various concentrations of DOX were incubated with cultures of 20,000 cells in 48-well tissue culture plates, as described above. The cement pods were submerged directly into the wells with low-serum culture medium. AlamarBlue assays were performed after 1, 4, and 7 days of cement treatment to determine metabolic activity. Live/Dead (Invitrogen, #L3224) cell viability/cytotoxicity stains were applied according to manufacturer instructions. Briefly, cell medium was removed and 100 μL of Live/Dead solution in PBS was added to the wells and incubated at 37°C for 15 min before being imaged with an EVOS M5000 imaging system (Invitrogen, #AMF5000). Similarly, cement samples were incubated with 2D cultures of hbmMSCs (RoosterBio Inc., Maryland, USA) and human osteoblasts isolated in our laboratory from lumbar spine tissues harvested from organ donors, as described previously (REB Protocol #2020-5647, approved by the institutional review board of McGill University) [31]. AlamarBlue assays were performed after 4 days and 7 days of treatment. Short tandem repeat (STR) identification was omitted for the primary osteoblasts as our focus on primary cells, despite potential heterogeneity, aligns with our goal of assessing treatment efficacy on a cell population representative of the intended target. Additionally, mycoplasma testing was not conducted on the cell lines and primary cell population in consideration of their reliable sourcing from reputable repositories with established quality controls, thereby mitigating the necessity for redundant testing and ensuring the integrity of our experimental design.

To assess the efficacy of the cement in 3D *in vitro* culture, MDA-MB-231 and C4-2B spheroids were formed by placing 20,000 cells in Nunclon Sphera round-bottom 96-well plates (Thermo Fisher Scientific, #174925) and centrifuging at 290× *g* for 3 min to form a pellet (day 0). On day 1, MDA-MB-231 pellets received 100 μL of a 4 μg/mL solution of ready-to-use bovine collagen I (Sigma-Aldrich, #5074) for a final concentration of 2 μg/mL and were centrifuged at 100× *g* for 3 min. C4-2B spheroids were ready on day 4 and MDA-MB-231 spheroids were ready on day 6. Once ready, the cell medium was discarded, and spheroids were coated with a 1:1 solution of low-serum cell culture medium and collagen I gel for a final collagen concentration of 2.5 mg/mL. Spheroids were considered ready once they were compact enough to tolerate the addition of the 2.5 mg/mL collagen solution without breaking apart. The plates were incubated at 37°C for 90 min for the gelation of the collagen. Following the gelation, the wells were topped with fresh low-serum cell culture medium. The following day, the spheroids in collagen gel were transferred to non-adherent 48-well plates containing low-serum cell culture medium, and the cement pods were juxtaposed

in the wells. A 2 μmol/L concentration of free DOX in cell medium served as a positive control. AlamarBlue assays were performed after 1, 4, and 7 days of cement treatment to determine metabolic activity, with a modified incubation time of 6 h. Live/Dead and 4',6-diamidino-2-phenylindole (DAPI; Invitrogen, #R37606) stains were applied according to manufacturer instructions. Fluorescence and phase contract images of the pellets were taken to visualize pellet size and cell migration into the collagen matrix. Area quantification was performed with ImageJ software (NIH, Maryland, USA).

Statistics

GraphPad Prism Version 9 (GraphPad Software, San Diego, California, USA) was used for statistical analyses. DOX release data were fitted with two-phase exponential association functions. The compounded standard error of the mean (SEM) was determined for DOX release data due to the propagation of error from repeated measurements of the same samples at various timepoints. Dose-response data were fitted using sigmoidal functions and relative half-maximal inhibitory concentration (IC_{50}) values were obtained with their 95% confidence intervals (CI). All data was assumed to have a normal distribution and thus two-way analysis of variances (ANOVAs) with Tukey's correction for multiple comparisons were performed to test for significance for parametric data. One-way ANOVAs with Tukey's correction were performed to compare differences in mechanical strength and SCA properties between groups. Experiments were run in triplicate and performed thrice for an N of 3, unless otherwise indicated. Significance was set at an P of 0.05. Where shown in-text, data are represented as mean ± SD. Graphical error bars are represented as SEM and ns indicates $P > 0.05$, * indicates $P < 0.05$, ** indicates $P < 0.01$, *** indicates $P < 0.001$, and **** indicates $P < 0.0001$.

Results

DOX-NP cement and release kinetics

Mesoporous silica NPs were loaded with DOX and mixed into PMMA bone cement. The cement was shaped into cylindrical pods with a diameter of 2.23 mm ± 0.08 mm and a height of 3.13 mm ± 0.07 mm. The addition of NPs to the cement created a network and altered the microstructure within the cement, creating pockets of NPs encapsulated by the cement (Figure 1). The polymer beads in the cement powder interconnected with the polymerization of the methylmethacrylate (MMA) and incorporated the NPs, fixing them in place. The cement containing 8% w/w NPs displayed a higher degree of connectivity between NPs compared to cement containing 2% w/w NPs.

The SCAs were measured from blank cement, as well as cement containing 2% and 8% w/w NPs (Figure 2). The SCA was 75.5° ± 3.4° for blank cement, 78.3° ± 3.2° for 2% w/w NP cement, and 74.4° ± 1.7° for 8% w/w NP cement, with no significant differences between the groups ($P > 0.05$).

The mechanical properties of cement were evaluated with the addition of NPs. Cylindrical samples of blank cement were prepared with a diameter of 6.03 mm ± 0.03 mm and a height of 12.00 mm ± 0.05 mm. Cement containing 2% w/w NPs was prepared with a diameter of 6.04 mm ± 0.03 mm and a height of 11.96 mm ± 0.11 mm. Cement containing 8% w/w NPs was prepared with a diameter of 6.12 mm ± 0.06 mm and a height of 11.98 mm ± 0.02 mm. Representative stress-strain curves are shown in Figure 3A. The Young's modulus for blank cement was determined to be 2,983 MPa ± 99 MPa, 2,533 MPa ± 154 MPa for 2% w/w NP cement and 3,024 MPa ± 90 MPa for 8% w/w NP cement, revealing a significant decrease in the cement containing 2% w/w NPs compared to the blank and 8% w/w NP cement (Figure 3B, $P < 0.05$). Furthermore, the ultimate compressive strength of blank cement was determined to be 120 MPa ± 4 MPa, 96 MPa ± 5 MPa for 2% w/w NP cement and 116 MPa ± 7 MPa for 8% w/w NP cement, with a significant decrease in the cement containing 2% w/w NPs compared to the blank and 8% w/w NP cement (Figure 3C, $P < 0.05$).

The release kinetics of DOX were evaluated in cement containing 2% and 8% w/w NPs, loaded with various amounts of DOX. The NPs retained between 77% and 93% of the DOX in the loading solution. At a given quantity of NPs, the proportion retained increased with increasing concentrations of DOX in the

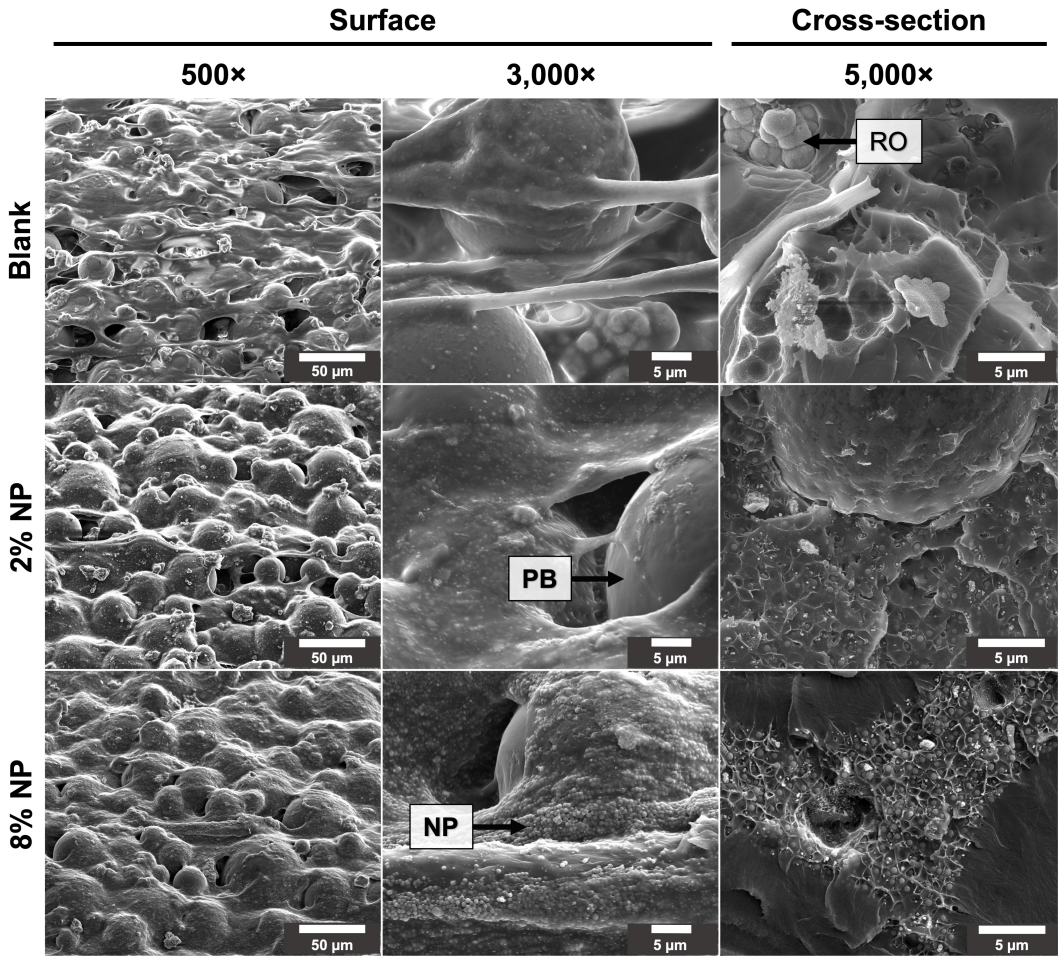

Figure 1. Surface and cross-sectional scanning electron microscope images of cement mixed without NPs (blank) and with 2% and 8% w/w NPs. RO: radioopacifier crystals [zirconium dioxide (ZrO_2)]; PB: PMMA polymer beads

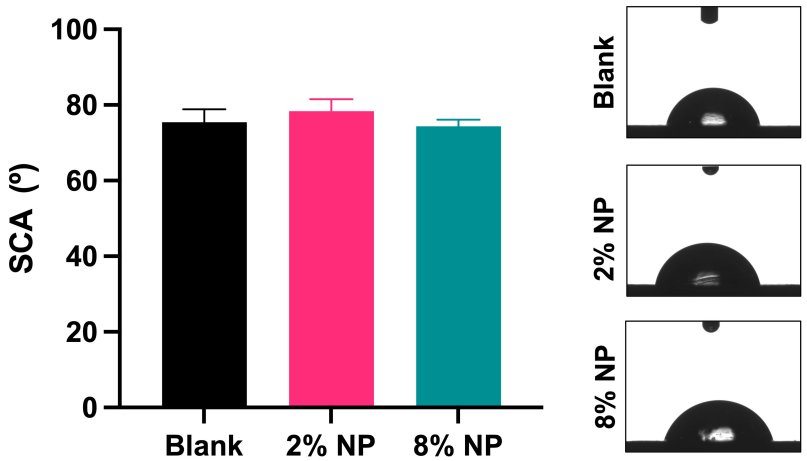

Figure 2. Static water contact angles and representative images of cement mixed without NPs (blank) and with 2% and 8% w/w NPs. *N* = 3. Error bars represent SD

loading solution (Figure 4A). Additionally, 40 mg of NPs were able to retain approximately 5% more DOX compared to 10 mg at a given loading concentration ($P = 0.0002$). When we assessed the ability of the PMMA cement alone (without NPs) to elute DOX, 240 nmol of DOX was mixed directly into cement without NPs. The release from this cement was limited, and a plateau was reached by day 4 (Figure 4B). With the addition of NPs, the release of DOX was facilitated with a significant increase in the cumulative DOX release at day 4 for the cement containing 8% w/w NPs ($P < 0.0001$). Furthermore, cement containing 8% w/w NPs had a significantly higher cumulative release on day 4 compared to the equivalent cement containing

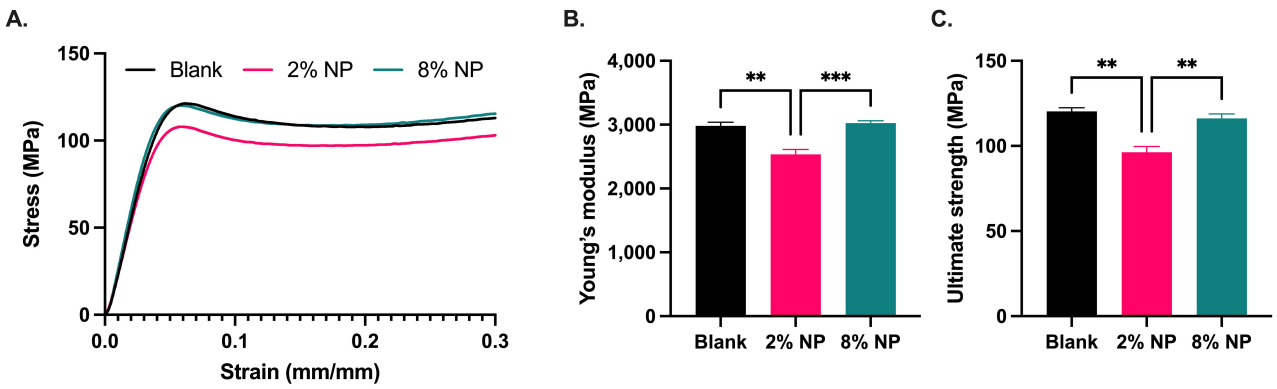

Figure 3. Cement compression testing. A. Stress-strain curves; B. Young's moduli; and C. ultimate compression strengths of cement containing no NPs (blank; *N* = 3), 2% and 8% w/w NPs (*N* = 5). Error bars represent SEM. ** indicates *P* < 0.01, *** indicates *P* < 0.001

2% w/w NPs (*P* = 0.0012). By day 28, the cement with 2% and 8% w/w NPs had released 3.1 times and 16.7 times more DOX, respectively, compared to the cement without NPs.

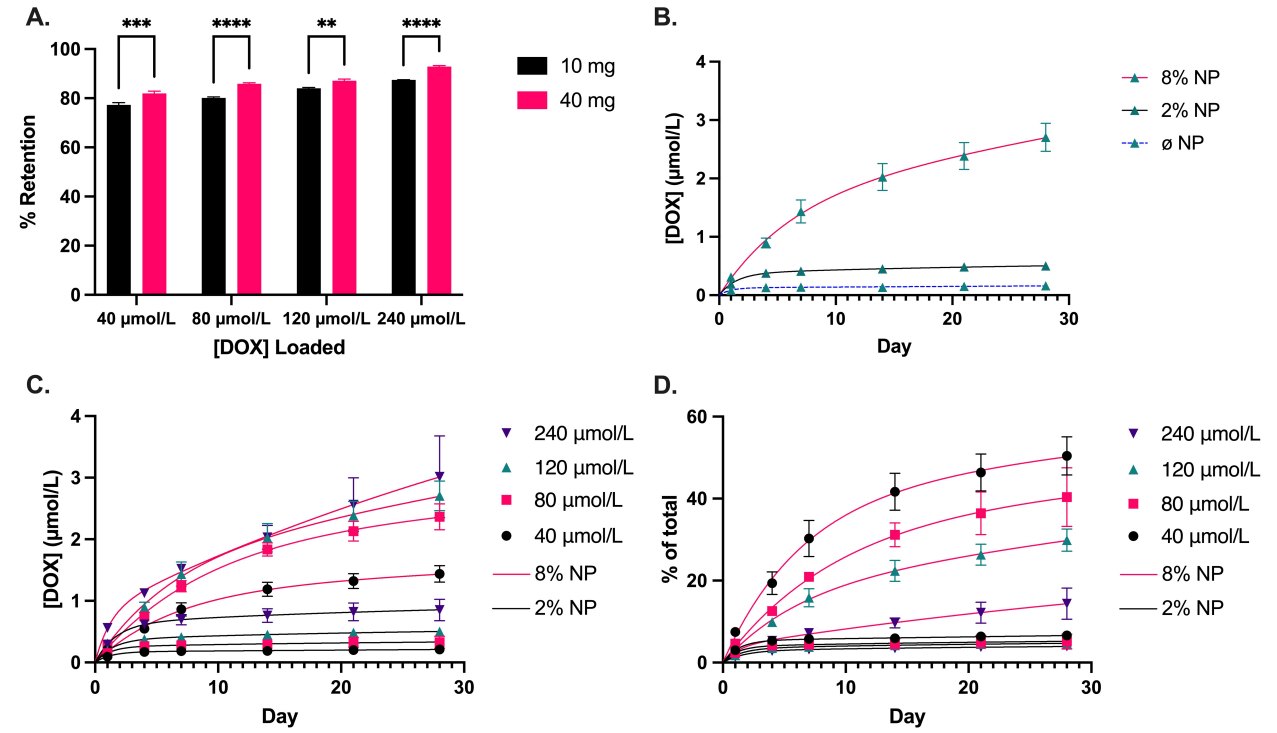

Figure 4. DOX loading and release profiles. A. Proportion of DOX retained by 10 mg and 40 mg of NPs at various loading concentrations of DOX, corresponding to 2% and 8% NP w/w mixed into the cement, respectively; B. DOX release from cement containing no NPs (Ø NP; *N* = 2), 2% and 8% w/w NPs loaded with an equivalent of 120 µmol/L of DOX; C. cumulative concentration; and D. proportional release of DOX over 28 days from cement containing 2% and 8% w/w NPs loaded with 40, 80, 120, and 240 µmol/L of DOX. Solid line: 2% w/w NP. Dashed line: 8% w/w NP. *N* = 3. Error bars represent SEM in (A) and compounded SEM for DOX release profiles in (B–D). ** indicates *P* < 0.01, *** indicates *P* < 0.001, and **** indicates *P* < 0.0001

The cumulative release of DOX was higher for the cement containing 8% w/w NPs compared to 2% w/w NPs at all concentrations of DOX as of day 7 (Figure 4C, *P* < 0.0001). Similarly, the proportional release of DOX was higher for the cement containing 8% w/w NPs compared to 2% w/w NPs (Figure 4D). However, there was no significant difference in the proportional release between the various concentrations for cement containing 2% w/w NPs, with an average proportional release rate of 0.037% per day over days 14–28. Conversely, there was a significant difference in the proportional release rates of DOX within the 8% w/w NP cement group. The cement containing NPs loaded with lower concentrations achieved a higher proportional release, as high as 50% in 28 days. The average proportional DOX release

rate for 8% w/w NP cement was 0.54% per day over days 14–28, or approximately 15 times higher compared to 2% w/w NP cement. Assuming a constant diffusion coefficient (D) for finite cylinders, the release kinetics are governed by the following:

$$\frac{M_t}{M_{tot}} = 1 - \sum_{n=1}^{\infty} \frac{4}{a^2\alpha_n^2} \exp(-D\alpha_n^2 t) \sum_{m=0}^{\infty} \frac{8}{l^2\beta_m^2} \exp(-D\beta_m^2 t) \quad (1)$$

Where, M_t is the mass of DOX released at time t, M_{tot} is the total mass of DOX in the sample, a is the radius and l is the height of the cylinder, aa_n is the nth zero of the zero-order Bessel function of the first kind where $J_0(aa_n) = 0$, and $\beta_m = \frac{(2m+1)\pi}{l}$. At later stages of release, only the first term in equation 1 will contribute and we obtain:

$$\frac{M_t}{M_{tot}} = 1 - \frac{32}{a^2 l^2 \alpha_1^2 \beta_0^2} \exp[-D(\alpha_1^2 + \beta_0^2)t] \quad (2)$$

Which gives us the following expression:

$$\ln(1 - M_t/M_{tot}) \propto -D(\alpha_1^2 + \beta_0^2)t \quad (3)$$

Thus, by plotting $\ln(1 - M_t/M_{tot})$ *versus* time (Figure 5), we are able to calculate the slope of the linear region to obtain the average diffusion coefficients for each cement composition: $D_{ø\ NP}$: 3.19 × 10^{-16} m^2/s, $D_{2\%\ NP}$: 7.92 × 10^{-16} m^2/s, and $D_{8\%\ NP}$: 1.64 × 10^{-14} m^2/s.

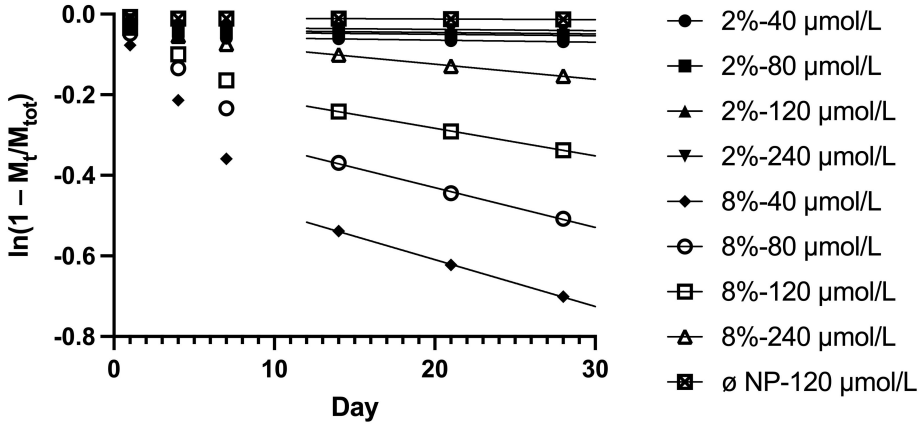

Figure 5. Plot of $\ln(1 - M_t/M_{tot})$ *versus* time, where M_t is the mass of DOX released at time t and M_{tot} is the total mass of DOX in the sample

2D *in vitro* efficacy assay

Both MDA-MB-231 and C4-2B cells treated with DOX for 7 days had higher IC_{50} values compared to cells treated for 3 days ($P < 0.05$). The IC_{50} curves are shown in Figure 6. The calculated IC_{50} values are indicated in Table 2. These IC_{50} values guided the selection of the loading concentrations of DOX for the NPs to achieve the release of effective drug doses.

The *in vitro* efficacy of the DOX-loaded NP cement was evaluated in monolayer cultures of MDA-MB-231 and C4-2B cells. On day 1, there was no significant difference between the treatments for both cell lines. After 4 days and 7 days of treatment, the metabolic activity of MDA-MB-231 cells was significantly reduced with the DOX cement formulations compared to the cement containing NPs without DOX (0 μmol/L; Figure 7A, $P < 0.05$). Furthermore, on day 4, the cement containing NPs loaded with 120 μmol/L of DOX was more effective than the 40 μmol/L formulation ($P = 0.0021$). There was no significant difference between the metabolic activities of MDA-MB-231 cells treated with cement with and without NPs (blank). C4-2B cells treated with 0 μmol/L cement had a lower metabolic activity on day 4 compared to blank cement (Figure 7B, $P < 0.05$). This difference was no longer significant on day 7. After 4 days and 7 days of

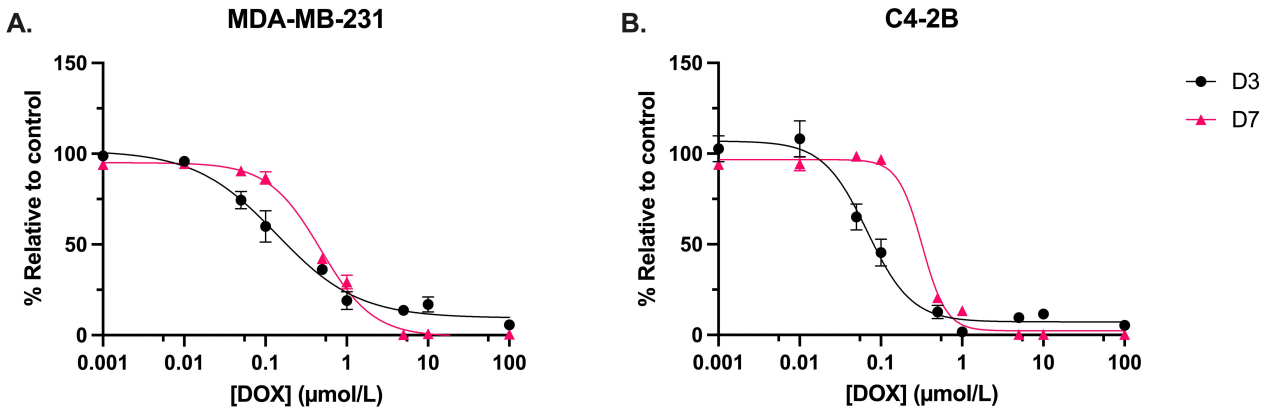

Figure 6. Dose-response curves evaluating the metabolic activity. A. MDA-MB-231 cells; and B. C4-2B cells. Treated with DOX for 3 days (D3) and 7 days (D7). *N* = 3. Error bars represent SEM

Table 2. IC_{50} values for DOX against MDA-MB-231 and C4-2B cell lines at D3 and D7, with 95% CI

Cell line	IC_{50}—D3 (μmol/L)	IC_{50}—D7 (μmol/L)
MDA-MB-231	0.14 (95% CI: 0.09, 0.21)	0.48 (95% CI: 0.41, 0.56)
C4-2B	0.07 (95% CI: 0.05, 0.09)	0.32 (95% CI: 0.26, 0.40)

D3: 3 days; D7: 7 days

treatment, the metabolic activity of C4-2B cells was significantly reduced with the DOX cement formulations compared to the 0 μmol/L cement ($P < 0.05$). Representative images of Live/Dead staining are shown in Figure 8. For both cell lines, a reduction in cell proliferation and viability on day 7 compared to day 1 is observed in cells treated with DOX cement.

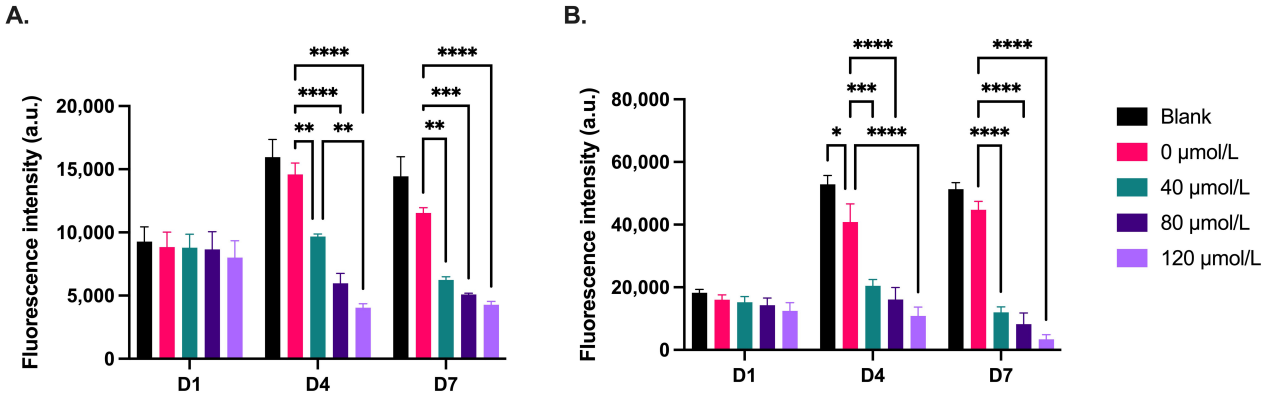

Figure 7. Metabolic activity of 2D cultures of (A) MDA-MB-231 and (B) C4-2B cell lines treated with cement constructs for 1 day (D1), 4 days (D4), and 7 days (D7). Blank: cement without NPs; 0 μmol/L: NP cement without DOX. *N* = 3. Error bars represent SEM

The cement's toxicity against healthy cells was assessed with 2D cultures of hbmMSCs and human osteoblasts derived from spinal tissue. At day 4 of treatment, the 80 μmol/L DOX cement formulation decreased the metabolic activity of hbmMSCs compared to the 0 μmol/L control (Figure 9A, $P = 0.0357$). At day 7, the 80 μmol/L DOX cement formulation decreased the activity of both hbmMSCs ($P = 0.0044$) and osteoblasts ($P = 0.0002$) compared to the control (Figure 9). The metabolic activity of hbmMSCs was not significantly different from day 4 to day 7 of treatment. However, the metabolic activity of the osteoblasts for all treatment groups was significantly higher on day 7 compared to day 4 (Figure 9B, $P < 0.0001$).

3D *in vitro* metabolic activity assay and pellet size quantification

To assess the *in vitro* efficacy of the DOX cement constructs in a more physiological cell culture system, metabolic activity, spheroid growth and cell outgrowth was assessed in 3D collagen-coated spheroid cultures. This method allowed for the concurrent evaluation of metabolic activity and cell migration. There

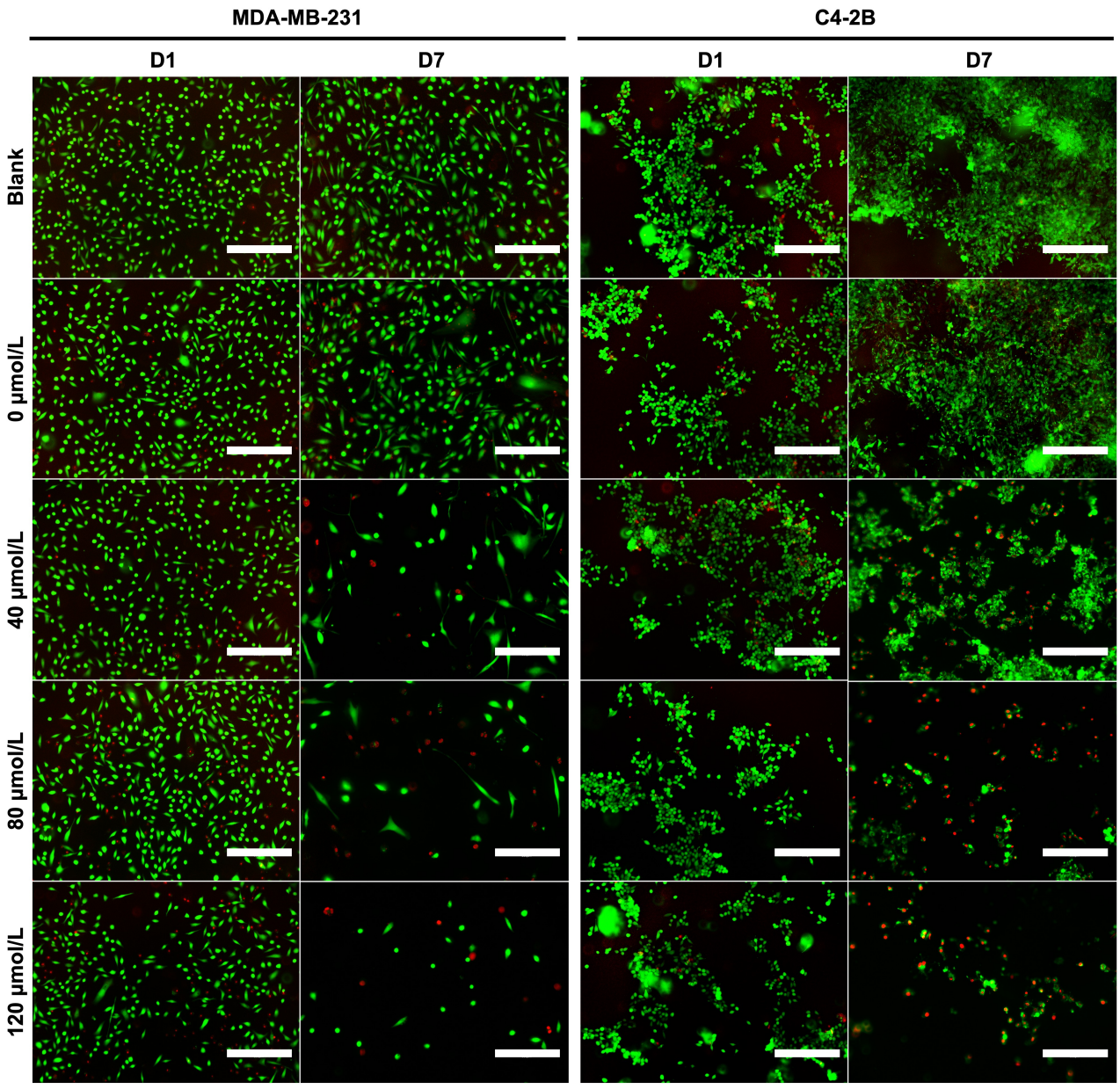

Figure 8. Representative Live/Dead staining images of MDA-MB-231 and C4-2B cells at day 1 (D1) and day 7 (D7) of treatment with cement constructs. Green: alive; red: dead. Scale bar = 300 μm

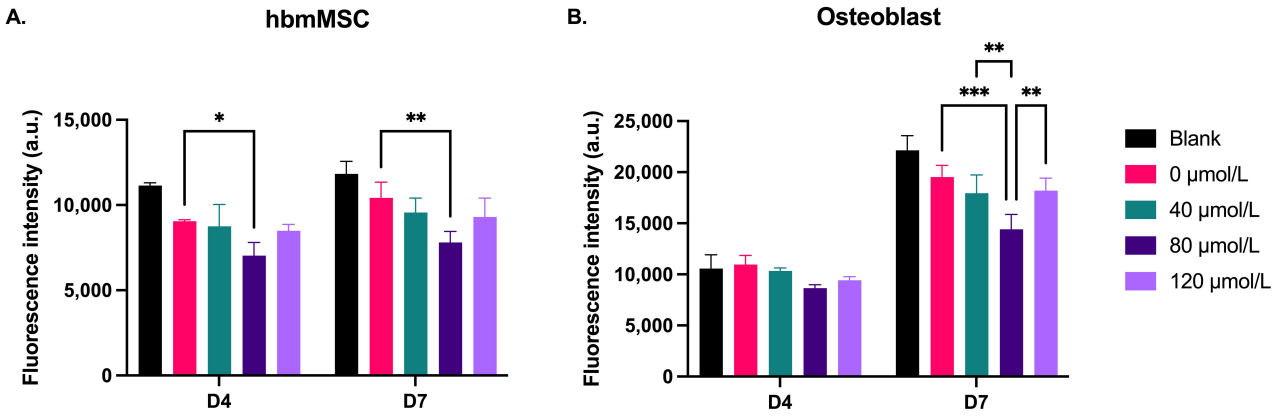

Figure 9. Metabolic activity of 2D cultures of (A) hbmMSCs and (B) osteoblasts treated with cement constructs for 4 days (D4) and 7 days (D7). Blank: cement without NPs. 0 μmol/L: NP cement without DOX. $N = 1$. Error bars represent SD. * indicates $P < 0.05$, ** indicates $P < 0.01$, *** indicates $P < 0.001$

was no significant difference in terms of metabolic activity and cell migration between treatments on day 1 for both MDA-MB-231 and C4-2B spheroids. On days 4 and 7, there was a significance reduction in metabolic activity of MDA-MB-231 spheroids treated with DOX cement, compared with the 0 μmol/L cement (Figure 10A, $P < 0.05$). On day 7, MDA-MB-231 spheroids treated with the 0 μmol/L displayed lower metabolic activity compared to the blank cement ($P = 0.0005$). The activity of C4-2B spheroids was significantly reduced with the 120 μmol/L composition on day 4, and with the 240 μmol/L composition on day 7 (Figure 10B, $P < 0.05$). The area of migrated MDA-MB-231 cells was significantly reduced on days 4 and 7 with the DOX cement, compared to the 0 μmol/L cement (Figure 10C, $P < 0.05$). By day 4, the 240 μmol/L cement formulation significantly reduced C4-2B spheroid size compared to the 0 μmol/L cement (Figure 10D, $P = 0.0057$). By day 7, both the 120 μmol/L and 240 μmol/L formulations were effective at inhibiting the growth of C4-2B spheroids (Figure 10D, $P < 0.05$). A high degree of cell migration was observed in the collagen-coated MDA-MB-231 spheroids from day 1 to 7 for the blank and 0 μmol/L cement treatments (Figure 11). Furthermore, the MDA-MB-231 spheroids displayed necrotic tumor cores on day 7 for all treatments and the spheroids treated with DOX appear to have gradually imploded, showing necrotic rings around the inner core. C4-2B spheroids did not display a high degree of cell migration but did show differences in overall spheroid size and compaction (Figure 12). The Live/Dead staining of the C4-2B spheroids treated with the DOX cement show the highest degree of cell death in the spheroid core, with a darker appearance overall with phase contrast imaging.

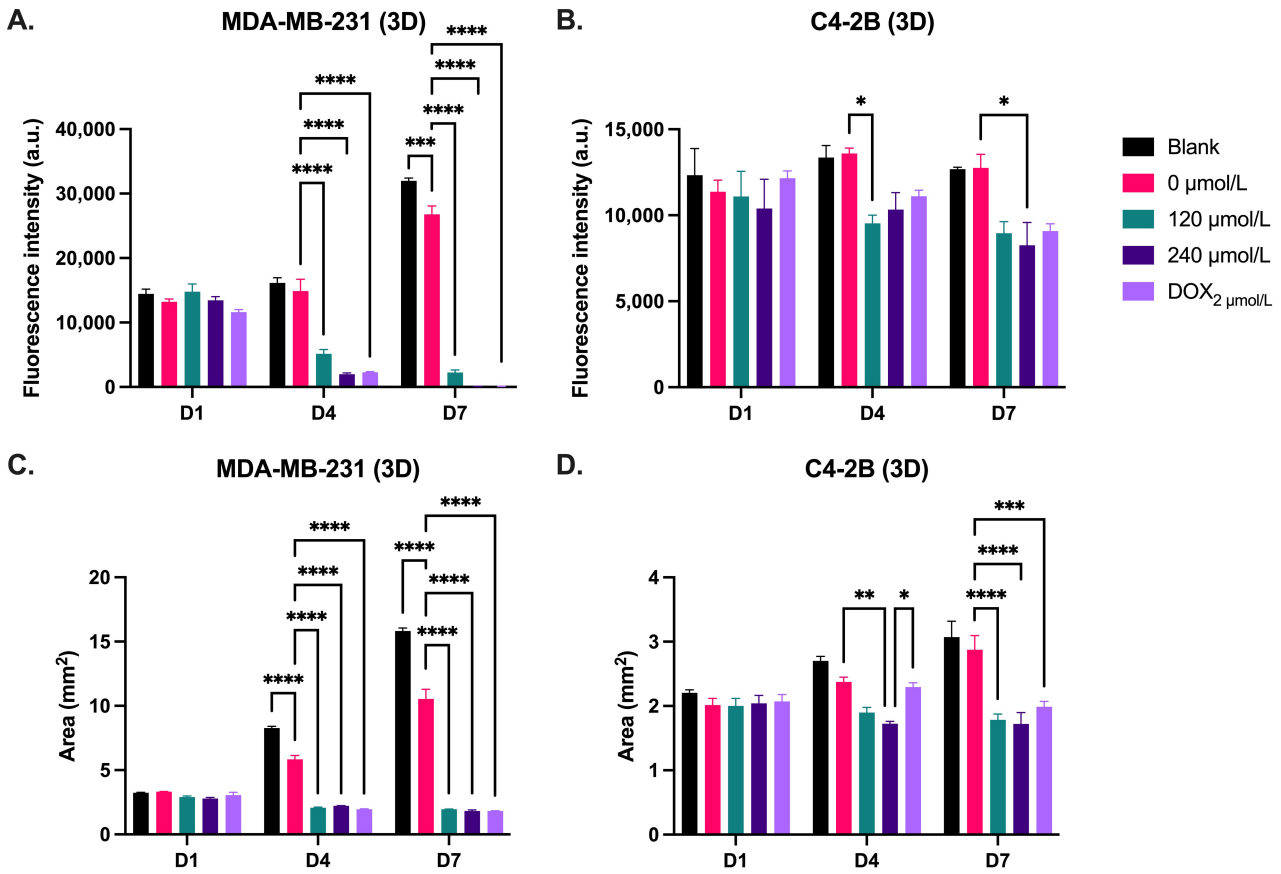

Figure 10. Metabolic activity and area of 3D spheroid cultures of (A, C) MDA-MB-231 and (B, D) C4-2B cell lines treated with cement constructs for 1 day (D1), 4 days (D4), and 7 days (D7). $DOX_{2\ \mu mol/L}$: free 2 μmol/L DOX treatment. $N = 3$. Error bars represent SEM. * indicates $P < 0.05$, ** indicates $P < 0.01$, *** indicates $P < 0.001$, and **** indicates $P < 0.0001$

2D *versus* 3D *in vitro* efficacy

On day 7 of treatment, MDA-MB-231 cells treated with control cement (0 μmol/L) in 3D culture had a 2.3-fold higher metabolic activity compared to cells in 2D culture (Figure 13A, $P < 0.0001$). There was no significant difference in MDA-MB-231 metabolic activity between 2D and 3D culture when treated with DOX cement. However, after a 7-day treatment with DOX cement, the activity of MDA-MB-231 cells was

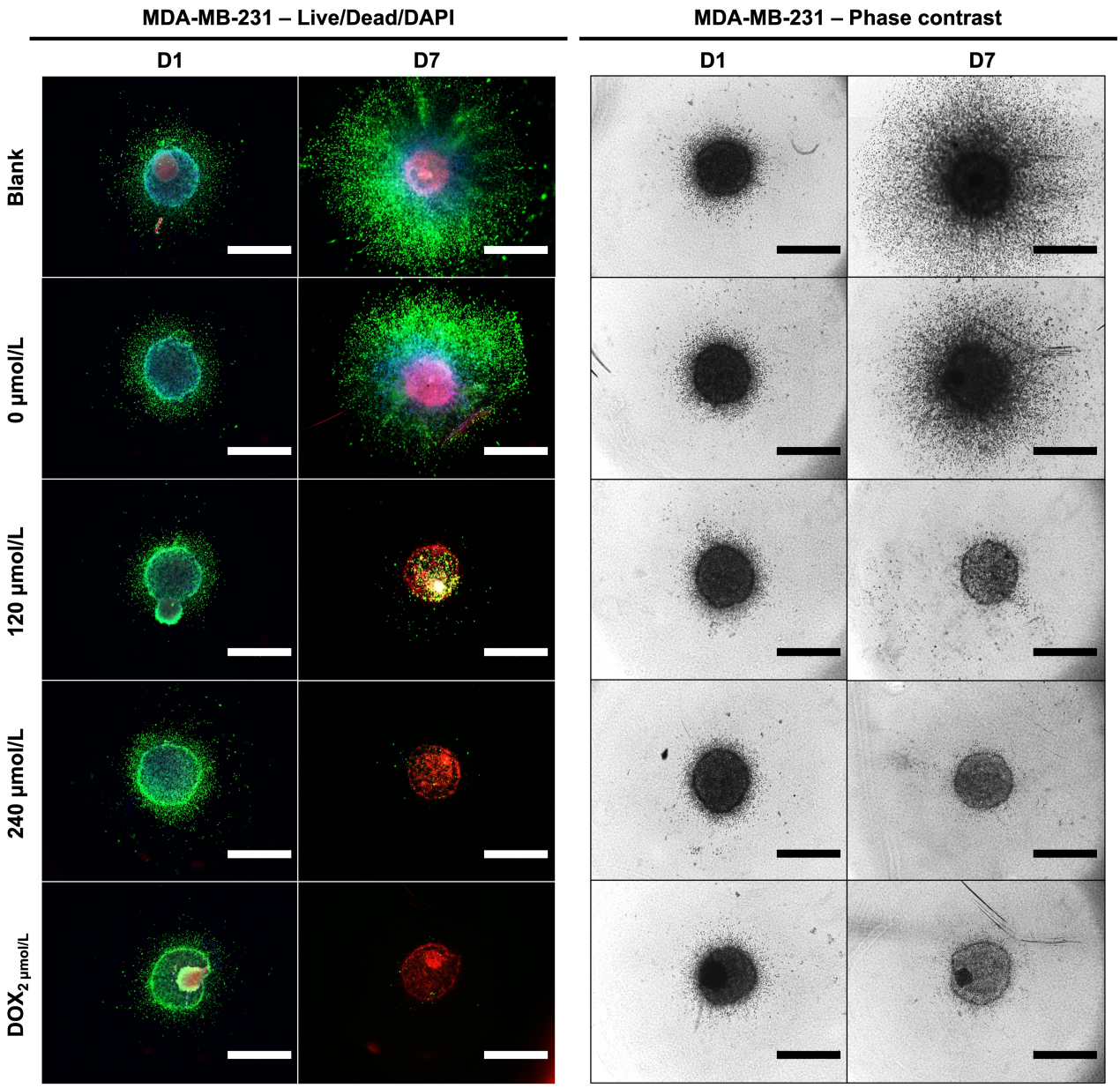

Figure 11. Representative Live/Dead/DAPI staining and phase contrast images of MDA-MB-231 cells at day 1 (D1) and day 7 (D7) of treatment with cement constructs. Green: alive; red: dead; blue: cell nuclei. Scale bar = 1,250 µm

reduced by 63% compared to control cement in 2D culture and by 92% in 3D culture, demonstrating an increased DOX efficacy in 3D culture against MDA-MB-231 cells. Conversely, C4-2B cells in 3D culture exhibited a 3.5-fold lower metabolic activity after 7 days compared to 2D culture (Figure 13B, $P < 0.0001$). There was no significant difference in C4-2B metabolic activity between 2D and 3D culture when treated with DOX cement for 7 days. However, after a 7-day treatment with DOX cement, the activity of C4-2B cells was reduced by 92% compared to control cement in 2D culture and by 30% in 3D culture, demonstrating a reduced DOX efficacy in 3D culture against the C4-2B cell line.

Discussion

The development of a bone cement with both mechanical integrity and controlled chemotherapeutic release is desirable for preventing local tumor recurrence after bone tumor resection surgeries. In the present study, we investigated the addition of DOX-loaded mesoporous silica NPs to PMMA bone cement. Specifically, we evaluated the compressive strength and wettability with the addition of NPs, the DOX release profiles as a function of loaded drug concentrations and NP content within the cement. We then

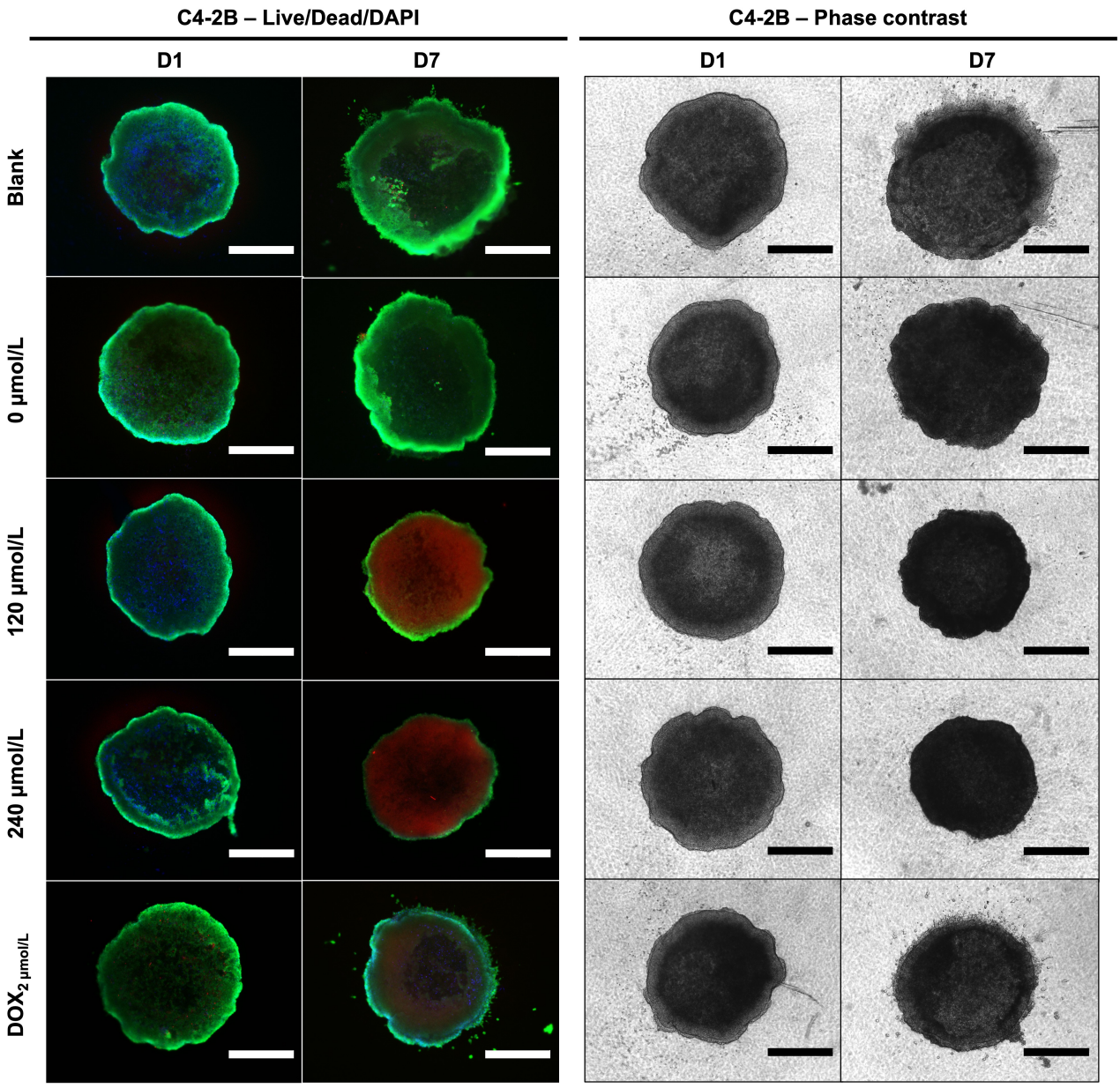

Figure 12. Representative Live/Dead/DAPI staining and phase contrast images of C4-2B cells at day 1 (D1) and day 7 (D7) of treatment with cement constructs. Green: alive; red: dead; blue: cell nuclei. Scale bar = 750 µm

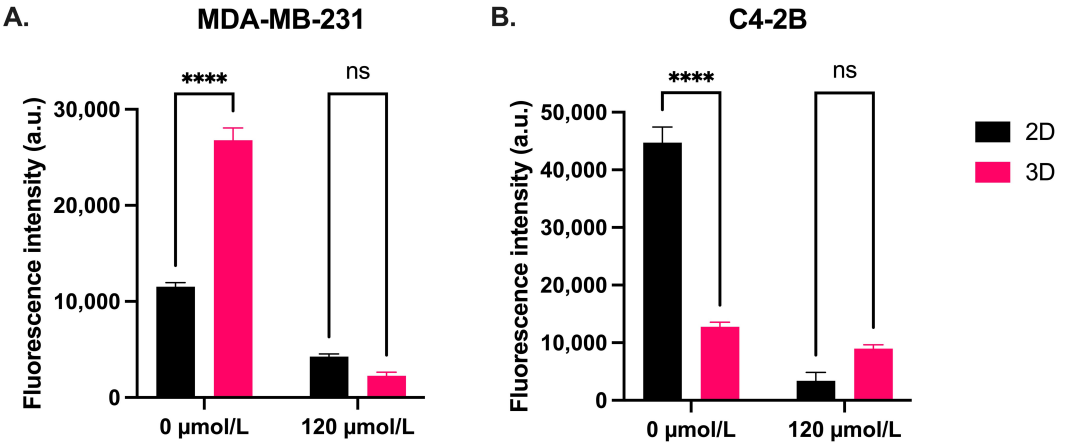

Figure 13. Comparison of the metabolic activity of (A) MDA-MB-231 and (B) C4-2B cells in 2D and 3D culture treated for 7 days with control cement (0 µmol/L) and cement containing NPs loaded with 120 µmol/L DOX. *N* = 3. Error bars represent SEM. ns indicates *P* > 0.05

assessed the *in vitro* efficacy of the cement in 2D and 3D cell cultures using breast and prostate cancer cell lines and compared drug sensitivities between 2D and 3D culture models. We also assessed the augmented cement's toxicity against healthy hbmMSCs and human osteoblasts.

With the addition of NPs to PMMA cement, scanning electron microscope imaging displayed a change in the microstructure of the cement. With a higher content of NPs in the cement, a higher degree of connectivity was observed between the NPs, leading to the formation of a nanonetwork within the cement. PMMA cements functionalized with mesoporous silica NPs require a certain concentration of NPs for the formation of a network that significantly improves drug elution [25]. Based on our drug elution profiles, the 2% NP w/w formulation only improved elution profiles slightly compared to the cement without NPs, with minor increases with increasing loaded concentration of DOX. With the 8% w/w NP composition, the elution rates had a higher dependence on the loaded concentration of the drug with a significantly improved elution rate. This indicates that a sufficient network had been formed to allow for the DOX to diffuse out from within the cement through the interconnected pores of the NPs. Furthermore, the contact angle measurements demonstrate that the addition of NPs to the PMMA did not alter the wettability of the cement. Taken together, the increased drug elution rates from the cement may be attributed to the formation of this nanoporous network allowing for enhanced diffusion, and not due to changes in hydrophobicity/hydrophilicity. Slane et al. [32] investigated the mechanical effects of the addition of mesoporous silica NP content in PMMA cement up to a content of 5% w/w. They determined that with increasing NP content, there was an increase in the flexural modulus, compressive strength, and compressive modulus. However, they observed a decrease in flexural strength, fracture toughness, and work to fracture [32]. We found that the addition of 8% w/w NPs to PMMA did not impact the ultimate compressive strength of the cement, nor the Young's (compressive) modulus, as the stress-strain curves were nearly identical. However, the addition of 2% w/w NPs to PMMA significantly reduced Young's modulus and the ultimate compressive strength of the cement. Studies investigating the mechanical properties of PMMA cements functionalized with mesoporous silica NPs are limited. Lee et al. [33] determined that at 5% w/w NPs, the flexural strength decreased in PMMA loaded with NPs with a diameter of 85 nm. Further investigation is required to elucidate the optimal range of NP content in PMMA cement with regards to mechanical properties. Similar to our findings for the 8% w/w NP cement, Letchmanan et al. [25] demonstrated that the addition of mesoporous silica NPs at 8.15% w/w into PMMA bone cement had negligeable effects on the compressive strength and flexural modulus even after 6 months of aging in PBS, and significantly increased the release of the loaded antibiotic, gentamicin. Furthermore, they show that more than 96% of the NPs loaded in PMMA were retained in the cement even after 6 months [25]. This demonstrates the feasibility of the NP cement for long-term load-bearing applications, such as in the case of the spine. PMMA cements can be modified with additives to increase their flexural strength and fracture toughness. Khaled et al. [34] utilized nanostructured titania fibers and determined that the addition of 1% w/w to PMMA significantly increased its flexural strength, flexural modulus, and fracture toughness. Studies evaluating the mechanical properties of multi-functionalized PMMA cements are necessary to develop a cement that can deliver long-term effective drug doses without compromising mechanical integrity.

It is thought that with the addition of NPs the enhanced drug release is achieved via the creation of a porous nanonetwork in the cement [25, 35, 36]. The mesoporous NPs themselves can hold large amounts of drugs within their pores due to the high surface area. As we increased the concentration of DOX in the loading solution for the NPs, the percentage of the DOX retained by the NPs also continued to increase. This indicates that the NPs had not yet been saturated with the drug at these concentrations. Furthermore, there was only a 5% increase in retention despite a 4-fold increase in the quantity of NPs. This demonstrates the exceptionally high capacity of mesoporous NPs to hold compounds within their pores. Shen et al. [37] determined that mesoporous NPs with a diameter of 120 nm and a pore size of 5.2 nm were capable of retaining DOX at a concentration of 306 mg/g of NPs, well beyond what we used in this study. The addition of NPs was required for the cement to release effectives doses of DOX in a sustained manner. Without NPs, a plateau was reached relatively quickly in the release profile. When a higher concentration of DOX was used

to load the NPs, they retained more of it and were also able to release it more. With a higher NP content in the cement, the diffusion of DOX was greater for all concentrations. The 2% NP w/w cement loaded with 240 μmol/L released less DOX than the 8% NP w/w cement loaded with 40 μmol/L, despite being loaded with a six-fold higher DOX concentration. This indicates that the drug elution rate from PMMA is largely determined by the NP content within the cement. The proportion of DOX released from the cement was highest for the cement containing the NPs loaded with the lowest concentration of DOX. This is likely due to the DOX closer to the proximity of the surface being eluted the quickest, and the diffusion from the center being the most difficult [38]. Given a 50% release of DOX in 28 days from the 8% NP w/w cement with the lowest DOX concentration, it is reasonable to postulate that the NP cements with higher amounts of DOX would simply take longer to liberate more DOX, allowing for a prolonged release. It is worth noting that within both 2% and 8% w/w NP cement groups, the diffusion coefficients decreased slightly with increasing loading concentrations. This may be due to the imperfect sink conditions in the method for determining the release kinetics. Nonetheless, the addition of NPs to the cement confers a greater mass diffusivity, with over a 50-fold increase with 8% w/w NPs in the cement compared to without, and over a 20-fold increase compared to 2% w/w NPs.

Consistent with our findings, PMMA with 10.19% NPs w/w loaded with DOX released 60% of the drug in a period of 60 days, whereas the cement without NPs plateaued at 5% of the loaded drug on the first day followed by negligeable release thereafter [36]. To increase the drug releases rates, Li et al. [39] functionalized mesoporous NPs with poly(acrylic acid). As a result, the NP drug release profiles were pH sensitive. The functionalized NPs released 70% of DOX in 6 days at pH 5.5, and 25.3% at pH 7.4 [39]. As tumor microenvironments are acidic (pH: 6.5–6.9) due to the high glycolytic rate of tumor cells [40, 41], mixing functionalized NPs such as these into PMMA cement would allow for a pH-controlled drug release, allowing for a tumor-responsive cement. Future work may evaluate the release profiles in terms of NP diameter, pore size, and functionalization.

To determine the optimal concentration ranges for DOX-NP loading, dose-response experiments were conducted on monolayer cultures of MDA-MB-231 and C4-2B cell lines. DOX IC_{50} values were determined for 3-day (72 h) incubation times for MDA-MB-231 and C4-2B cell lines, shown in Table 2. These values were comparable to those in the literature [42, 43]. Additionally, the 7-day (168 h) IC_{50} values were reported to evaluate drug resistance. As seen in Figure 6, both cell lines display higher cell metabolic activities at the mid-range doses when treated with DOX for 7-days, indicating that the cells are more resistant. Han et al. [44] observed that the number of MDA-MB-231 cells exposed to mid-range DOX concentrations had increased after 8 days of treatment, demonstrating their ability to proliferate in a tolerable DOX concentration range. They concluded that the DOX resistance is associated with epigenetic alterations in histone deacetylase, and that suberoylanilide hydroxamic acid (SAHA; a histone deacetylase inhibitor) restored DOX sensitivity [44]. This is an important consideration for a cement intended for a sustained drug release profile, as the dose must be high enough to avoid chemoresistance. Agents such as SAHA can be incorporated into the cement to increase the sensitivity of the tumor cells to the chemotherapy drug. Tonak et al. [45] combined SAHA with valproic acid mixed directly into PMMA for the local treatment of osteosarcoma. Similarly, Koto et al. [46] directly incorporated the third-generation bisphosphonate, zoledronic acid, into PMMA cement and the resulting cement exhibited antitumor effects against multiple malignant tumor cell types without systemic toxicity *in vivo*.

When incubated with both 2D and 3D cultures of MDA-MB-231 and C4-2B cell lines, a time- and dose-dependent inhibition of the cancer cells was observed with the DOX-NP cement formulations. In 2D culture, the metabolic activities of both cell lines were inhibited with all DOX-NP cement formulations as of day 4 and maintained at day 7. On day 4 of treatment, C4-2B cells showed a lower metabolic activity when treated with the 0 μmol/L NP cement, compared to the blank cement. However, on day 7 this difference was no longer significant. It is possible that the addition of the NPs to the cement facilitated the release of the MMA monomer in the cement. Unpolymerized MMA leakage from PMMA has been demonstrated to have cytotoxic effects on human cells, and PMMA cement has been shown to have a cytotoxic effect against metastatic spine cells [47–49]. For both cell lines, Live/Dead imaging from 2D culture displays a reduction

in the density of living cells and an increase in dead cells with the DOX-NP cement treatment, as compared to the 0 μmol/L and blank controls. Most studies have been conducted with chemotherapy drug powders mixed directly into PMMA. Furthermore, the method used to test the cement *in vitro* varies between studies. Many studies have mixed methotrexate, DOX, and cisplatin directly into PMMA and incubated the cement samples with cell medium, and then treated cells with the medium containing the drugs eluted from the cement. As the release kinetics reach their peak quickly due to a burst release, efficacy against cancer cells decreases over time [19, 50, 51]. Cyphert et al. [27] recently used this indirect incubation method to test their DOX-loaded polymeric γ-cyclodextrin microparticle PMMA cement. They determined that PMMA loaded with 15% w/w DOX-microparticles had consistent cytotoxic effects over time, compared to cement with DOX mixed directly into it. This can be attributed to the more consistent release of the drug from the composite cement, relative to the burst release in the control cement without microparticles. However, the addition of 15% w/w microparticles to the cement decreased its ultimate compressive strength below the ISO 5833:2002 standard minimum threshold of 70 MPa [27]. In our study, a direct incubation method was used where the DOX-NP cement samples were incubated directly with the cells submersed in the cell medium, similar to Özben et al. [52], which may be more indicative of the *in vivo* application. The treatment of hbmMSCs and osteoblasts with DOX-NP cement resulted in minimal effects compared with the cancer cell lines. With treatment, the general trend of the metabolic activity of the cancer cell lines was to decrease from day 1 to day 7. However, the overall activity of the hbmMSCs did not change from day 4 to day 7, whereas it increased for the osteoblasts in all treatment groups. This demonstrates the selectivity of the DOX-NP cement for the highly proliferative cell types.

In 3D culture, the metabolic activity and overall spheroid area was assessed in response to cement treatment. As tumors *in vivo* grow in a 3D environment, standard 2D cultures are unable to accurately simulate the native tumor microenvironment. Therefore, more physiologically relevant 3D models, such as spheroids, are increasingly being used for drug screening [53, 54]. Spheroids are characterized by proliferative (outer), quiescent (middle), and necrotic (inner) cell layers due to nutrient, gas, and pH gradients. They also generally possess higher drug resistances compared to standard monolayer cultures [55]. For the MDA-MB-231 cell line, a similar trend in 3D was observed as in 2D culture, where all the DOX-NP cement samples significantly reduced inhibited the metabolic activity of the spheroids. MDA-MB-231 spheroids have been shown to form loose spheroids and have similar drug sensitivities in 2D as they do in 3D culture [56]. Indeed, the MDA-MB-231 spheroids demonstrate an abundant proliferative zone as the tumor cells migrated outwards along the collagen matrix. The area of spheroids treated with the control blank and 0 μmol/L cements increased over the period of 7 days, whereas the DOX-NP cement treatments inhibited cell migration completely. A necrotic core is visible in the center of the control spheroids, as expected, due to the limited availability of nutrients and gas exchange in the core. With DOX-NP cement treatments, MDA-MB-231 spheroids showed dead cells and a reduced cell density as seen on phase contrast imaging. The C4-2B spheroids were more resistant to the DOX-NP cement treatment, compared to 2D culture. Mosaad et al. [57] evaluated the metabolic activity of C4-2B spheroids in response to docetaxel and found that they were more resistant compared to 2D culture. In contrast to the MDA-MB-231 spheroids, the C4-2B spheroids did not display an abundant outgrowth of cells. However, DOX-NP cement treatments reduced the size of the spheroids compared to control cement. Live/Dead imaging revealed a significant red fluorescent zone in the C4-2B spheroids treated with DOX-NP cement after 7 days. Spheroids treated with a free DOX concentration of 2 μmol/L in cell medium did not display the same degree of ethidium accumulation (red signal) in cells at the core. As the metabolic activity of the C4-2B spheroids was not drastically different between the treatment groups, it is unlikely that the fluorescent red signal is associated with dead cells from the Live/Dead staining. Rather, it may reflect the accumulation of DOX within the spheroid, which displays a red autofluorescence. A red fluorescent protein (RFP) filter cube was used for the fluorescence microscopy, which can also detect DOX [58]. Based on the DOX release kinetics, an estimated 1.5 μmol/L concentration should have been achieved in the cell medium by day 7. However, as the medium was not changed for the duration of the experiments, the pH drop may have increased the release kinetics leading to a higher dose of DOX and thereby causing more DOX accumulation in the

spheroids. Furthermore, the metabolic activity of control C4-2B spheroids does not significantly increase over the course of the 7-day experiment, nor does the area increase as much as it does for the MDA-MB-231 spheroids. Future experiments could focus on determining the actual DOX uptake under these experimental conditions.

In comparing 2D and 3D cultures, a difference in the metabolic activities can be seen between the culture methods for the control spheroids. At day 7, MDA-MB-231 spheroids demonstrated a significantly higher metabolic activity in 3D culture, whereas C4-2B spheroids were significantly less active in 3D culture. Although there was no statistically significant difference between culture models for the DOX-NP cement treatment, the relative inhibition of MDA-MB-231 cells was higher in 3D culture, whereas it was higher in 2D culture for C4-2B cells. C4-2B spheroids have been reported to undergo moderate growth for the first 5–7 days, followed by a plateau in the proliferation rate [57]. Another prostate cancer cell line, PC3, has been shown to remain quiescent and proliferate slowly in 3D spheroid culture [59]. In contrast, spheroids formed with the highly invasive MDA-MB-231 cell line have been shown to grow rapidly over a period of 10 days [60]. As DOX targets rapidly dividing cells, it is expected that less proliferative or quiescent cells would be less affected by it [61]. This demonstrates the importance of 3D culture models for adequate high-throughput drug screening applications.

The limitations of the present study lie predominantly in the methods of predicting DOX release kinetics and the usage of cell lines. Predicting DOX release kinetics *in vivo* is challenging due to the differences in temperature, pH, medium used (e.g., PBS), etc. As release rates are determined by diffusion, the presence of concentration gradients can impact elution rates. In our assays, half the solution volume was replenished at each time point. In the *in vivo* case, however, DOX can diffuse into the entire organism, which may accelerate the release. Further experiments with various sink conditions are required to characterize release rates as a function of sink volumes and fractional replenishments. Established cell lines were used in this study for *in vitro* experiments, which may not accurately reflect spine metastatic cells. Future *in vitro* studies utilizing patient-derived spine metastatic cells in 3D culture would accurately predict the clinical success of our augmented PMMA cement. Nevertheless, our *in vitro* assessment in 2D and 3D culture showcases the efficacy of the DOX-NP cement for inhibiting cancer cell activity and migration. To our knowledge, no previous study has investigated the addition of chemotherapy-loaded mesoporous silica NPs to PMMA bone cement. Furthermore, *in vitro* efficacy of PMMA cement was assessed in 3D spheroid culture for the first time. Future work may assess combination chemotherapeutics for improved efficacy, various sizes of NPs and their functionalization for a better control of drug release profiles, as well as additional additives such as nanofibers to improve mechanical strength.

Abbreviations

2D: two-dimensional

3D: three-dimensional

CI: confidence intervals

DAPI: 4',6-diamidino-2-phenylindole

DOX: doxorubicin

hbmMSCs: human bone-marrow derived mesenchymal stem cells

IC_{50}: half-maximal inhibitory concentration

ISO: International Organization for Standardization

NPs: nanoparticles

Ø NP: doxorubicin without nanoparticles

PBS: phosphate-buffered saline

PMMA: polymethylmethacrylate

SAHA: suberoylanilide hydroxamic acid

SCA: static contact angles

SD: standard deviations

SEM: standard error of the mean

Declarations

Acknowledgments

The authors gratefully acknowledge Professor M. Park (McGill university) for providing donating a cell line used in this study and the support of the McGill Orthopaedic fellows and surgeons of the McGill Scoliosis and Spine Group for their assistance in obtaining primary human osteoblasts.

Author contributions

AS: Conceptualization, Data curation, Formal analysis, Investigation, Methodology, Validation, Visualization, Writing—original draft, Writing—review & editing. MMG and MEC: Investigation, Writing—original draft, Writing—review & editing. MHW and DHR: Conceptualization, Funding acquisition, Project administration, Resources, Writing—review & editing, Supervision. All authors read and approved the submitted version.

Conflicts of interest

The authors declare that they have no conflicts of interest.

Ethical approval

Human lumbar vertebral tissues were obtained from donors with institutional ethical approval in collaboration with Transplant Quebec. This study complies with the Declaration of Helsinki.

Consent to participate

Informed consent to participate in the study was obtained from all participants.

Consent to publication

Not applicable.

Availability of data and materials

The raw data supporting the conclusions of this manuscript will be made available by the authors, without undue reservation, to any qualified researcher.

Funding

AO Spine Young Investigator Research Grant Award 2022 [S-16-138W] awarded to DHR and MHW; Cancer Research Society operating grant 2018-2020 given to MHW; AS received the CIHR CGS-M and FRQS doctoral [318974] scholarships; MEC received the CIHR postdoctoral fellowship award [171258]; DHR is a FRQS Junior 2 Research Scholar. The funders had no role in study design, data collection and analysis, decision to publish, or preparation of the manuscript.

References

1. Barzilai O, Fisher CG, Bilsky MH. State of the art treatment of spinal metastatic disease. Neurosurgery. 2018;82:757–69.

2. Harel R, Angelov L. Spine metastases: current treatments and future directions. Eur J Cancer. 2010;46: 2696–707.
3. Liang T, Wan Y, Zou X, Peng X, Liu S. Is surgery for spine metastasis reasonable in patients older than 60 years? Clin Orthop Relat Res. 2013;471:628–39.
4. Sciubba DM, Gokaslan ZL. Diagnosis and management of metastatic spine disease. Surg Oncol. 2006; 15:141–51.
5. Rothrock RJ, Barzilai O, Reiner AS, Lis E, Schmitt AM, Higginson DS, et al. Survival trends after surgery for spinal metastatic tumors: 20-year cancer center experience. Neurosurgery. 2021;88:402–12.
6. Kurisunkal V, Gulia A, Gupta S. Principles of management of spine metastasis. Indian J Orthop. 2020; 54:181–93.
7. Bate BG, Khan NR, Kimball BY, Gabrick K, Weaver J. Stereotactic radiosurgery for spinal metastases with or without separation surgery. J Neurosurg Spine. 2015;22:409–15.
8. Howell EP, Williamson T, Karikari I, Abd-El-Barr M, Erickson M, Goodwin ML, et al. Total *en bloc* resection of primary and metastatic spine tumors. Ann Transl Med. 2019;7:226.
9. Hayashi K, Tsuchiya H. The role of surgery in the treatment of metastatic bone tumor. Int J Clin Oncol. 2022;27:1238–46.
10. Healey JH, Shannon F, Boland P, DiResta GR. PMMA to stabilize bone and deliver antineoplastic and antiresorptive agents. Clin Orthop Relat Res. 2003;415:S263–75.
11. Cloyd JM, Acosta FL Jr, Polley MY, Ames CP. En bloc resection for primary and metastatic tumors of the spine: a systematic review of the literature. Neurosurgery. 2010;67:435–45.
12. Roedel B, Clarençon F, Touraine S, Cormier E, Molet-Benhamou L, Le Jean L, et al. Has the percutaneous vertebroplasty a role to prevent progression or local recurrence in spinal metastases of breast cancer? J Neuroradiol. 2015;42:222–8.
13. Sundaresan N, Rothman A, Manhart K, Kelliher K. Surgery for solitary metastases of the spine: rationale and results of treatment. Spine (Phila Pa 1976). 2002;27:1802–6.
14. Ismat A, Walter N, Baertl S, Mika J, Lang S, Kerschbaum M, et al. Antibiotic cement coating in orthopedic surgery: a systematic review of reported clinical techniques. J Orthop Traumatol. 2021;22: 56.
15. Mensah LM, Love BJ. A meta-analysis of bone cement mediated antibiotic release: overkill, but a viable approach to eradicate osteomyelitis and other infections tied to open procedures. Mater Sci Eng C Mater Biol Appl. 2021;123:111999.
16. Wall V, Nguyen TH, Nguyen N, Tran PA. Controlling antibiotic release from polymethylmethacrylate bone cement. Biomedicines. 2021;9:26.
17. Lilikakis A, Sutcliffe MP. The effect of vancomycin addition to the compression strength of antibiotic-loaded bone cements. Int Orthop. 2009;33:815–9.
18. Hernigou P, Thiéry JP, Benoit J, Voisin MC, Leroux P, Hagege G, et al. Methotrexate diffusion from acrylic cement. Local chemotherapy for bone tumours. J Bone Joint Surg Br. 1989;71:804–11.
19. Rosa MA, Maccauro G, Sgambato A, Ardito R, Falcone G, De Santis V, et al. Acrylic cement added with antiblastics in the treatment of bone metastases. Ultrastructural and *in vitro* analysis. J Bone Joint Surg Br. 2003;85:712–6.
20. Phull SS, Yazdi AR, Ghert M, Towler MR. Bone cement as a local chemotherapeutic drug delivery carrier in orthopedic oncology: a review. J Bone Oncol. 2020;26:100345.
21. Handal JA, Tiedeken NC, Gershkovich GE, Kushner JA, Dratch B, Samuel SP. Polyethylene glycol improves elution properties of polymethyl methacrylate bone cements. J Surg Res. 2015;194:161–6.
22. Funk GA, Burkes JC, Cole KA, Rahaman MN, McIff TE. Antibiotic elution and mechanical strength of PMMA bone cement loaded with borate bioactive glass. J Bone Jt Infect. 2018;3:187–96.

23. Méndez JA, Abraham GA, del Mar Fernández M, Vázquez B, San Román J. Self-curing acrylic formulations containing PMMA/PCL composites: properties and antibiotic release behavior. J Biomed Mater Res. 2002;61:66–74.
24. Shen SC, Letchmanan K, Chow PS, Tan RBH. Antibiotic elution and mechanical property of TiO_2 nanotubes functionalized PMMA-based bone cements. J Mech Behav Biomed Mater. 2019;91:91–8.
25. Letchmanan K, Shen SC, Ng WK, Kingshuk P, Shi Z, Wang W, et al. Mechanical properties and antibiotic release characteristics of poly(methyl methacrylate)-based bone cement formulated with mesoporous silica nanoparticles. J Mech Behav Biomed Mater. 2017;72:163–70.
26. Kweon C, McLaren AC, Leon C, McLemore R. Amphotericin B delivery from bone cement increases with porosity but strength decreases. Clin Orthop Relat Res. 2011;469:3002–7.
27. Cyphert EL, Kanagasegar N, Zhang N, Learn GD, von Recum HA. PMMA bone cement composite functions as an adjuvant chemotherapeutic platform for localized and multi-window release during bone reconstruction. Macromol Biosci. 2022;22:e2100415.
28. Thorn CF, Oshiro C, Marsh S, Hernandez-Boussard T, McLeod H, Klein TE, et al. Doxorubicin pathways: pharmacodynamics and adverse effects. Pharmacogenet Genomics. 2011;21:440–6.
29. Krukiewicz K, Zak JK. Biomaterial-based regional chemotherapy: local anticancer drug delivery to enhance chemotherapy and minimize its side-effects. Mater Sci Eng C Mater Biol Appl. 2016;62: 927–42.
30. Sábio RM, Meneguin AB, Ribeiro TC, Silva RR, Chorilli M. New insights towards mesoporous silica nanoparticles as a technological platform for chemotherapeutic drugs delivery. Int J Pharm. 2019;564: 379–409.
31. Fairag R, Rosenzweig DH, Ramirez-Garcialuna JL, Weber MH, Haglund L. Three-dimensional printed polylactic acid scaffolds promote bone-like matrix deposition *in vitro*. ACS Appl Mater Interfaces. 2019;11:15306–15.
32. Slane J, Vivanco J, Meyer J, Ploeg HL, Squire M. Modification of acrylic bone cement with mesoporous silica nanoparticles: effects on mechanical, fatigue and absorption properties. J Mech Behav Biomed Mater. 2014;29:451–61.
33. Lee JH, El-Fiqi A, Jo JK, Kim DA, Kim SC, Jun SK, et al. Development of long-term antimicrobial poly(methyl methacrylate) by incorporating mesoporous silica nanocarriers. Dent Mater. 2016;32: 1564–74.
34. Khaled SM, Charpentier PA, Rizkalla AS. Physical and mechanical properties of PMMA bone cement reinforced with nano-sized titania fibers. J Biomater Appl. 2011;25:515–37.
35. Shen SC, Ng WK, Shi Z, Chia L, Neoh KG, Tan RB. Mesoporous silica nanoparticle-functionalized poly(methyl methacrylate)-based bone cement for effective antibiotics delivery. J Mater Sci Mater Med. 2011;22:2283.
36. Shen SC, Ng WK, Dong YC, Ng J, Tan RB. Nanostructured material formulated acrylic bone cements with enhanced drug release. Mater Sci Eng C Mater Biol Appl. 2016;58:233–41.
37. Shen J, He Q, Gao Y, Shi J, Li Y. Mesoporous silicananoparticles loading doxorubicin reverse multidrug resistance: performance and mechanism. Nanoscale. 2011;3:4314–22.
38. Cyphert EL, Learn GD, Marques DW, Lu CY, von Recum HA. Antibiotic refilling, antimicrobial activity, and mechanical strength of PMMA bone cement composites critically depend on the processing technique. ACS Biomater Sci Eng. 2020;6:4024–35.
39. Li H, Yu H, Zhu C, Hu J, Du M, Zhang F, et al. Cisplatin and doxorubicin dual-loaded mesoporous silica nanoparticles for controlled drug delivery†. RCS Adv. 2016;6:94160–9.
40. Feng L, Dong Z, Tao D, Zhang Y, Liu Z. The acidic tumor microenvironment: a target for smart cancer nano-theranostics. Natl Sci Rev. 2018;5:269–86.

41. Estrella V, Chen T, Lloyd M, Wojtkowiak J, Cornnell HH, Ibrahim-Hashim A, et al. Acidity generated by the tumor microenvironment drives local invasion. Cancer Res. 2013;73:1524–35.
42. Alkaraki A, Alshaer W, Wehaibi S, Gharaibeh L, Abuarqoub D, Alqudah DA, et al. Enhancing chemosensitivity of wild-type and drug-resistant MDA-MB-231 triple-negative breast cancer cell line to doxorubicin by silencing of STAT 3, Notch-1, and β-catenin genes. Breast Cancer. 2020;27:989–98.
43. Ni J, Cozzi P, Hao J, Beretov J, Chang L, Duan W, et al. Epithelial cell adhesion molecule (EpCAM) is associated with prostate cancer metastasis and chemo/radioresistance via the PI3K/Akt/mTOR signaling pathway. Int J Biochem Cell Biol. 2013;45:2736–48.
44. Han J, Lim W, You D, Jeong Y, Kim S, Lee JE, et al. Chemoresistance in the human triple-negative breast cancer cell line MDA-MB-231 induced by doxorubicin gradient is associated with epigenetic alterations in histone deacetylase. J Oncol. 2019;2019:1345026.
45. Tonak M, Becker M, Graf C, Eckhard L, Theobald M, Rommens PM, et al. HDAC inhibitor-loaded bone cement for advanced local treatment of osteosarcoma and chondrosarcoma. Anticancer Res. 2014;34: 6459–66.
46. Koto K, Murata H, Sawai Y, Ashihara E, Horii M, Kubo T. Cytotoxic effects of zoledronic acid-loaded hydroxyapatite and bone cement in malignant tumors. Oncol Lett. 2017;14:1648–56.
47. Chiang CC, Hsieh MK, Wang CY, Tuan WH, Lai PL. Cytotoxicity and cell response of preosteoblast in calcium sulfate-augmented PMMA bone cement. Biomed Mater. 2021;16:055014.
48. Fang J, Shen J, Jiang W, Dong W, Hu Z. Cytotoxicity of polymethyl methacrylate cement on primary cultured metastatic spinal cells. Mol Cell Toxicol. 2016;12:125–32.
49. Moreau MF, Chappard D, Lesourd M, Montheard JP, Basle MF. Free radicals and side products released during methylmethacrylate polymerization are cytotoxic for osteoblastic cells. J Biomed Mater Res. 1998;40:124–31.
50. Greco F, de Palma L, Specchia N, Jacobelli S, Gaggini C. Polymethylmethacrylate-antiblastic drug compounds: an *in vitro* study assessing the cytotoxic effect in cancer cell lines-a new method for local chemotherapy of bone metastasis. Orthopedics. 1992;15:189–94.
51. Maccauro G, Cittadini A, Casarci M, Muratori F, De Angelis D, Piconi C, et al. Methotrexate-added acrylic cement: biological and physical properties. J Mater Sci Mater Med. 2007;18:839–44.
52. Özben H, Eralp L, Baysal G, Cort A, Sarkalkan N, Özben T. Cisplatin loaded PMMA: mechanical properties, surface analysis and effects on Saos-2 cell culture. Acta Orthop Traumatol Turc. 2013;47: 184–92.
53. Fitzgerald AA, Li E, Weiner LM. 3D culture systems for exploring cancer immunology. Cancers (Basel). 2021;13:56.
54. Zanoni M, Piccinini F, Arienti C, Zamagni A, Santi S, Polico R, et al. 3D tumor spheroid models for *in vitro* therapeutic screening: a systematic approach to enhance the biological relevance of data obtained. Sci Rep. 2016;6:19103.
55. Carvalho MP, Costa EC, Miguel SP, Correia IJ. Tumor spheroid assembly on hyaluronic acid-based structures: a review. Carbohydr Polym. 2016;150:139–48.
56. Imamura Y, Mukohara T, Shimono Y, Funakoshi Y, Chayahara N, Toyoda M, et al. Comparison of 2D- and 3D-culture models as drug-testing platforms in breast cancer. Oncol Rep. 2015;33:1837–43.
57. Mosaad EO, Chambers KF, Futrega K, Clements JA, Doran MR. The microwell-mesh: a high-throughput 3D prostate cancer spheroid and drug-testing platform. Sci Rep. 2018;8:253.
58. Yildiz T, Gu R, Zauscher S, Betancourt T. Doxorubicin-loaded protease-activated near-infrared fluorescent polymeric nanoparticles for imaging and therapy of cancer. Int J Nanomedicine. 2018;13: 6961–86.
59. Hsiao AY, Torisawa YS, Tung YC, Sud S, Taichman RS, Pienta KJ, et al. Microfluidic system for formation of PC-3 prostate cancer co-culture spheroids. Biomaterials. 2009;30:3020–7.

60. Saraiva DP, Matias AT, Braga S, Jacinto A, Cabral MG. Establishment of a 3D co-culture with MDA-MB-231 breast cancer cell line and patient-derived immune cells for application in the development of immunotherapies. Front Oncol. 2020;10:1543.
61. van der Zanden SY, Qiao X, Neefjes J. New insights into the activities and toxicities of the old anticancer drug doxorubicin. FEBS J. 2021;288:6095–111.